WPS2-PR(18) 20436

D Lpez Bruna et al.

# Flux-surface averaged radial transport in toroidal plasmas with magnetic islands

Preprint of Paper to be submitted for publication in
Nuclear Fusion

This work has been carried out within the framework of the EUROfusion Consortium and has received funding from the Euratom research and training programme 2014-2018 under grant agreement No 633053. The views and opinions expressed herein do not necessarily reflect those of the European Commission.

This document is intended for publication in the open literature. It is made available on the clear understanding that it may not be further circulated and extracts or references may not be published prior to publication of the original when applicable, or without the consent of the Publications Officer, EUROfusion Programme Management Unit, Culham Science Centre, Abingdon, Oxon, OX14 3DB, UK or e-mail Publications.Officer@euro-fusion.org

Enquiries about Copyright and reproduction should be addressed to the Publications Officer, EUROfusion Programme Management Unit, Culham Science Centre, Abingdon, Oxon, OX14 3DB, UK or e-mail Publications.Officer@euro-fusion.org

The contents of this preprint and all other EUROfusion Preprints, Reports and Conference Papers are available to view online free at http://www.euro-fusionscipub.org. This site has full search facilities and e-mail alert options. In the JET specific papers the diagrams contained within the PDFs on this site are hyperlinked

# Flux-surface averaged radial transport in toroidal plasmas with magnetic islands

**D López-Bruna[1], B Momo[2], I Predebon[2], A López-Fraguas[1], F Auriemma[2], Y Suzuki[3] and R. Lorenzini[2]**

1 Laboratorio Nacional de Fusión – CIEMAT, 28040 Madrid, Spain
2 Consorzio RFX, corso Stati Uniti 4, 35127 Padova, Italy
3 National Institute for Fusion Science, National Institutes of Natural Sciences, Toki, Gifu 509-5292, Japan

**Abstract.** In toroidal magnetic confinement fusion research, one-dimensional (1D) transport models rely on one radial coordinate that labels nested toroidal flux surfaces. The presence of magnetic islands in the magnetic geometry does not impede making 1D transport calculations if the island regions are excluded and then, if necessary, treated separately. In this work we show a simple way to modify the flux-surface coordinate and corresponding metric coefficients when an island region is excluded. Comparison with the metrics obtained from Poincaré plots are shown, as well as applications to two types of plasma: Heliac (TJ-II, CIEMAT, Spain), where the geometrical effects alone cannot explain the experimental results when islands move throughout minor radius; and Heliotron (LHD, NIFS, Japan), where we estimate the effect of an island heat sink in flux-gradient relations.

## 1. Introduction

One dimensional (1D) transport codes, often referred to as "one-and-a-half D" because the metric coefficients are flux surface averaged (FSA), are widespread tools to interpret and analyze experimental data, and also to check transport theories. Assuming fair predictability is eventually achieved, 1D transport codes can become fundamental pieces of real-time plasma control in a fusion reactor. However, even if plasma transport theories reach such maturity, geometrical issues might still be a severe limitation to 1D codes in some important circumstances, namely, whenever there is a "considerable change" in the topology of the assumed set of nested toroids. As is well known, the 1D geometry based on the existence of flux surfaces is always broken at small enough spatial scales [1]. By "considerable change" we mean that calculations that use the ideal magnetic surface nesting and calculations that consider the broken geometry will differ, say, beyond the experimental precision. For example, MHD equilibrium codes such as VMEC [2] are often used to obtain magnetic configurations under the assumption of magnetic-surface nesting despite the presence of magnetic islands chains in the plasma. But an island chain bridges plasma regions through its separatrix, so the evaluation of transport will be considerably inaccurate when the plasma volume occupied by the islands is not negligible. This will be so, due to geometrical reasons, even if the transport properties outside the separatrix remain unchanged. In addition to the geometrical modifications, the presence of magnetic

islands may bring up notable modifications to the radial electric field that should be considered in transport calculations even in axisymmetric systems (see [3] and references therein).

The effect of magnetic islands on transport is evidently deleterious in many circumstances in tokamak plasmas, for example when large tearing modes develop. There are, however, many experimental indications that the development and dynamics of transport barriers is favored in the close vicinity of low order rational values of the rotational transform $\iota = 1/q$ (e.g. [4, 5, 6]), maybe due to the robustness of particular *irrational* values of $\iota$ near the resonances [7]. This is also true in currentless devices like stellarators (e.g. [8] and references therein). Therefore, a proper estimation of transport in plasmas where magnetic islands associated to low order rationals are present should be another common piece of transport codes. So far, the effects of such low order rationals in transport have been modeled in a few cases considering that transport increases near the resonant region, as in W7-AS [9]. On the other hand, many experiments in the TJ-II heliac suggest that a better description should be a *reduced* diffusivity around the resonant region [10, 11]; and magnetic island structures in the reverse-field device RFX can be associated to reduced transport [12]. Given the different magnetic geometries and plasma parameters of these devices, the effect of magnetic resonances on transport is clearly an open theoretical and experimental aspect in magnetic fusion research. This work concentrates on the geometrical aspects by extending the use of 1D transport codes to magnetic configurations with developed islands. Such tools might be necessary, for example, in the analysis of W7-X discharges, where magnetic islands must be considered not only as the basis of the island-divertor concept, but also as a possible transport element [13].

Transport with 1D codes relies on the existence of one radial coordinate generally related with flux surfaces in the whole plasma domain, which excludes the possibility of dealing with island regions. In this paper we propose a simple model to modify the metric coefficients that affect radial transport when the island (or maybe stochastic) region is excluded from the calculations. In essence, the original radial coordinate is mapped onto a new one that labels flux surfaces outside the island region. Therefore, the plasma volume occupied by the islands is eliminated from the calculations and the metric coefficients must change accordingly. Transport in the island region can be solved separately if needed. In order to explain these concepts we organize the paper as follows: Section 2 explains how to modify the metric coefficients when an island chain is taken away from the calculations (2.2), and then shows a comparison with FSA metric obtained directly from Poincaré plots (2.3). Section 3 shows two examples of application of the model based on TJ-II (3.2) and LHD (3.3) magnetic configurations where some physical conclusions are proposed. The paper is briefly summarized in Section 4.

## 2. Modification of the flux-surface averaged metric coefficients in presence of magnetic islands

### *2.1. Basic idea*

As is well known, a radius-like coordinate $\rho_0$ in a confining toroidal magnetic field can be defined under the hypothesis of nested toroidal magnetic surfaces. A magnetic island chain impedes the definition of a *single* flux-surface radial coordinate for

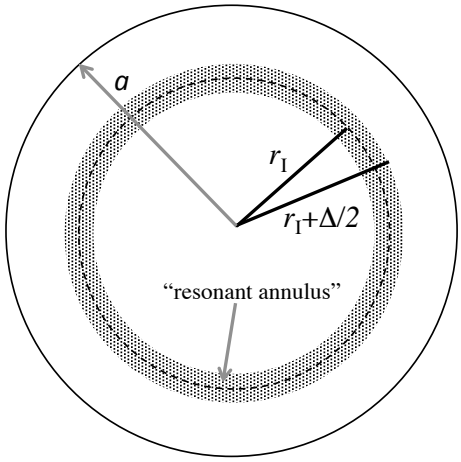


**Figure 1.** Circular cross section of an ideal torus with minor radius $a$ and resonant region of radial width $\Delta$ around $r = r_I$. The annulus represents a resonant layer occupied by islands. A uniform magnetic field with toroidal component $B_0$ is assumed. Taken from [14].

the entire plasma. The magnetic surfaces can still be labelled but a coordinate transformation from $\rho_0$ cannot be defined in the whole plasma domain. On the other hand, if the island region is *excluded*, we recover the possibility of having a useful radial coordinate $\rho$, i.e., a continuous and monotonous transformation $\rho(\rho_0)$ exists in the new domain. Since a portion of volume is taken away, this must be a piecewise transformation. An evident example of new coordinate is the enclosed volume as follows: the flux surfaces from the original magnetic axis to the inside portion of the separatrix provide a coordinate in that region, while from the outside part of the separatrix to the plasma edge we keep on adding also the enclosed volume discounting the island one. The space integral of the Jacobian of each transformation yields the enclosed volume in each portion.

To help in fixing ideas, let us suppose a cylindrical column where the magnetic island chain is represented by a centered annulus of width $\Delta$ around radius $r = r_\mathrm{I}$ (see sketch in figure 1). Outside the annulus we want to define a new label $\rho(r)$ that is continuous and keeps the normalization $\rho(r = a) = 1$. For continuity we require $\rho(r-\Delta/2) = \rho(r+\Delta/2)$. Since it will be useful later, let us relate our new coordinate with the enclosed toroidal flux due to a homogeneous magnetic field $B_0$ transverse to the cross-section. Then, for the normalization we discount the toroidal flux through the annulus,

$$\Phi_\mathrm{I} = B_0\pi\left[\left(r_\mathrm{I}+\frac{\Delta}{2}\right)^2-\left(r_\mathrm{I}-\frac{\Delta}{2}\right)^2\right] = B_0\pi 2 r_\mathrm{I}\Delta. \tag{1}$$

A simple choice of coordinate for the new plasma domain consists of defining, at the respective sides of the annulus,

**Inside part:** Square root of the flux $B_0\pi r^2$ normalized to $B_0\pi a^2 - \Phi_\mathrm{I}$;

**Outside part:** Square root of the flux $B_0\pi r^2 - \Phi_\mathrm{I}$ normalized to $B_0\pi a^2 - \Phi_\mathrm{I}$.

Substituting Eq. 1 we immediately obtain the transformations

$$\rho = \begin{cases} \sqrt{\frac{r^2}{a^2-2r_{\rm I}\Delta}};\ r < r_{\rm I} - \frac{\Delta}{2} \\ \sqrt{\frac{r^2-2r_{\rm I}\Delta}{a^2-2r_{\rm I}\Delta}};\ r > r_{\rm I} + \frac{\Delta}{2}. \end{cases}$$

Next we generalize this simple example considering that an original toroidal flux is given with associated FSA metric quantities.

### *2.2. Annular model*

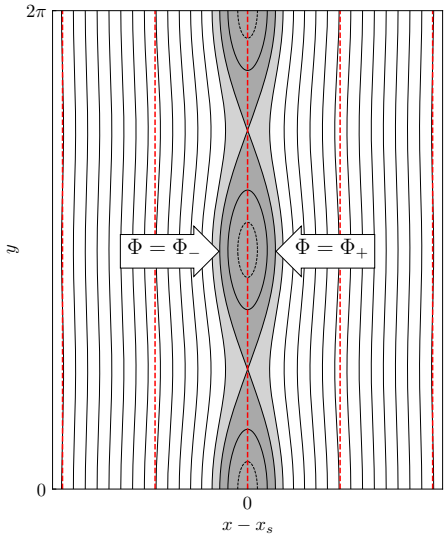


**Figure 2.** Sketch, in slab geometry, of unperturbed (red lines, only a few are drawn for clarity) and perturbed (black lines) flux surfaces when an island chain opens around a resonant position $x = x_s$. The islands region (dark grey) is limited by the separatrix, which can be divided in inside and outside parts enclosing respectively the perturbed fluxes $\Phi_-$ and $\Phi_+$. In a region covering the islands (light grey) a function $\Phi(x, y)$ can still be defined to provide a radial coordinate, but without the meaning of enclosed toroidal flux.

Let us begin by assuming magnetic configurations with a well defined flux-surface coordinate $\rho_0 = \sqrt{\Phi_0/\Phi_{0a}}$ in the whole plasma domain, where $\Phi_0(\mathbf{x})$ represents the usual enclosed toroidal flux and $\Phi_{0a}$ is the value at any point of the last closed flux surface. A low order rational of $\iota$ is found at $\rho_{0s} = \sqrt{\Phi_{0s}/\Phi_{0a}}$. The opening of islands around $\rho_{0s}$ deforms the nearby toroidal flux surfaces, but we can still define a coordinate $\bar{\rho}_0 = \sqrt{\Phi/\Phi_{0a}}$ through a function $\Phi(\mathbf{x})$ playing the role of enclosed toroidal flux as follows. For a given $\mathbf{x}$ we have $\Phi = \Phi_0$ far and $\Phi \approx \Phi_0$ closer to the island separatrix. This is illustrated in figure 2 with a sketch in slab geometry where, as usual, we associate $x$ to the minor radius and $y$ to the poloidal angle in a torus. Far from the resonant position, $x_s$, the perturbed flux (black lines) is practically like the unperturbed one (red lines) and we can define a function $\Phi = \Phi_0$. Closer to the separatrix, but not yet in the shaded region, we can use a function $\Phi(x, y) \approx \Phi_0(x, y)$ that adjusts to the real flux surfaces and keeps the meaning of enclosed toroidal flux. In the shaded region (light grey) covering the islands (dark grey) we can always

define toroidal surfaces with associated values $\Phi \approx \Phi_0$ in order to have a coordinate $\bar{\rho}_0(\rho_0)$, but the meaning will no longer be "enclosed toroidal flux". For example, we can impose $\bar{\rho}_{0s} \equiv \rho_{0s}$ for some surface that contains the island O and X points like the unperturbed flux at $x = x_s$. More generally, if $\Phi_\mathrm{I}$ is the toroidal flux through the islands cross-section, we assume a monotonous relation such that $\bar{\rho}_0 \to \rho_0$ when $\Phi_\mathrm{I} \to 0$. Conceptually, it is on this new coordinate $\bar{\rho}_0$ that we apply the piecewise transformation due to eliminating $\Phi_\mathrm{I}$. By analogy with the elimination of the flux through the cylindrical annulus in figure 1, we define

$$\rho = \begin{cases} \sqrt{\frac{\Phi}{\Phi_{0a}-\Phi_\mathrm{I}}};\ \Phi < \Phi_- \equiv \text{ toroidal flux before inside separatrix} \\ \sqrt{\frac{\Phi-\Phi_\mathrm{I}}{\Phi_{0a}-\Phi_\mathrm{I}}};\ \Phi > \Phi_+ \equiv \text{ toroidal flux after outside separatrix} \end{cases} \tag{2}$$

where we assume an idealized single-helicity island chain with its separatrix consisting on two surfaces: inside (facing the plasma center) and outside (facing plasma edge) separatrices connected at the X-point lines. It is convenient to define both sides of the separatrix in the $\bar{\rho}_0$ coordinate

$$\bar{\rho}_{0\mp} \equiv \sqrt{\frac{\Phi_\mp}{\Phi_{0a}}} \equiv \sqrt{\frac{\Phi_{0s} \mp \Phi_\mathrm{I}/2}{\Phi_{0a}}}, \tag{3}$$

with which the transformations Eq. 2 become

$$\rho = \begin{cases} \gamma\bar{\rho}_0;\ \bar{\rho}_0 < \bar{\rho}_{0-} \\ \gamma\bar{\rho}_0\sqrt{1-\beta^2/\bar{\rho}_0^2};\ \bar{\rho}_0 > \bar{\rho}_{0+} \end{cases} \tag{4}$$

having defined the parameters

$$\beta^2 \equiv \frac{\Phi_\mathrm{I}}{\Phi_{0a}} < 1 \tag{5}$$

$$\gamma \equiv \sqrt{\frac{1}{1-\beta^2}} \geq 1. \tag{6}$$

Recalling $\bar{\rho}_{0s} = \sqrt{\Phi_{0s}/\Phi_{0a}}$ we write 3 as $\bar{\rho}_{0\mp} = \sqrt{\bar{\rho}_{0s}^2 \mp \beta^2/2}$ to easily see that the transformations 4 guarantee a unique $\rho(\bar{\rho}_{0-}) = \rho(\bar{\rho}_{0+}) \equiv \rho_s$. The inverse transformation is

$$\bar{\rho}_0 = \begin{cases} \rho\gamma^{-1};\ \rho < \rho_s \\ \rho\gamma^{-1}\sqrt{1+\gamma^2\beta^2/\rho^2};\ \rho > \rho_s. \end{cases} \tag{7}$$

Metric coefficients only related with the radial coordinate are based on the derivative

$$\frac{\mathrm{d}\rho}{\mathrm{d}\bar{\rho}_0} = \begin{cases} \gamma \\ \gamma/\sqrt{1-\beta^2/\bar{\rho}_0^2} \end{cases}. \tag{8}$$

The modification of the metric is due to $\beta^2$, which is proportional to the width $\Delta$ of the resonant annulus in the cylindrical case, Eq. 1. Since the purpose now is just having a parameter for the island effect, we do not need any formulation to estimate $\beta^2$ but adopt instead the cylindrical prescription $\Phi_\mathrm{I}/\Phi_{0a} = 2r_\mathrm{I}\Delta/a^2$. Substituting $r_\mathrm{I} = a\bar{\rho}_{0s}$ we set

$$\beta^2 = \frac{2\bar{\rho}_{0s}\Delta}{a}, \tag{9}$$

where $a$ is the effective minor radius of the original configuration without islands.

In general, 1D transport calculations are done on some "flux surface" coordinate that is found even if the original magnetic fields (e.g. obtained from Poincaré plots)

include small-width magnetic island regions. Applying the transformation Eq. 4 to these configurations is like considering that the magnetic flux surfaces are not deformed by the presence of the islands even near the separatrix. Additionally, equation 9 parameterizes the island-enclosed toroidal flux by the annulus width according to figure 1. For these reasons we refer to the model as "annular". Strictly speaking, then, the ideal unperturbed coordinate $\rho_0$ does not exist and we can consider $\bar{\rho}_0$ as the coordinate representing the configurations without islands. Now, in terms of $\bar{\rho}_0$:

- Typical equilibrium coordinates used in 1D transport codes can be considered as $\bar{\rho}_0$, an approximation of a real configuration where small magnetic islands may be present. Then the piecewise transformation $\rho(\bar{\rho}_0)$ in Eq. 4 allows for a first approximation to the opening of a significant island chain.
- A dimensional radial coordinate can be defined using the effective minor radius of the unperturbed configuration: $r = a\rho(\bar{\rho}_0)$.
- Only Eq. 8 is needed to define the new metric coefficients from the metric that characterizes the equilibrium without islands:

$$\frac{\mathrm{d}V}{\mathrm{d}\rho} = \frac{\mathrm{d}V}{\mathrm{d}\bar{\rho}_0}\frac{\mathrm{d}\bar{\rho}_0}{\mathrm{d}\rho} \tag{10}$$

$$\nabla\rho = \frac{\mathrm{d}\rho}{\mathrm{d}\bar{\rho}_0}\nabla\bar{\rho}_0 \tag{11}$$

$$g^{\rho\rho} = \left(\frac{\mathrm{d}\rho}{\mathrm{d}\bar{\rho}_0}\right)^2 g^{\bar{\rho}_0\bar{\rho}_0}. \tag{12}$$

  For simplicity we drop the notation for FSA although all gradients are flux-surface averaged. Note, however, that this refers only to radial transport. The evolution of the plasma current density, for example, includes other metric coefficients not treated here, like $g^{\theta\theta}$ for the poloidal angle.
- The transformation Eq. 4 implies discontinuities in the radial fluxes. The transport code must be able to deal with them; or, else, it must be checked that the smoothing of the discontinuities provoked by the finite-difference numerical scheme does not alter the results significantly.
- The magnitude $V' \equiv \mathrm{d}V/\mathrm{d}\rho$ (Eq. 10) is continuous if the specific volume is proportional to the original coordinate, $\mathrm{d}V/\mathrm{d}\bar{\rho}_0 \propto \bar{\rho}_0$, which is a common case and always a choice for $\bar{\rho}_0$. This is easy to find by noting that $\bar{\rho}_0\bar{\rho}_0' = \rho/\gamma^2$ for all $\rho$ (here $\bar{\rho}_0' \equiv \mathrm{d}\bar{\rho}_0/\mathrm{d}\rho$).
- Excluding the islands, as expressed in the transformation Eq. 4, excludes the separatrix (otherwise there would be bi-valuated functions). The point representing the separatrix is, however, included in the transport problem by simply imposing its condition of common boundary, i.e., $\partial_t|_{\rho\to\rho_s} = \partial_t|_{\rho_s} = \partial_t|_{\rho_s\leftarrow\rho}$.

We end this section with two important remarks. First, observe that if discontinuities in the fluxes are allowed then the transport in the island region can be solved separately and taken into account as an additional term in the discontinuities of the fluxes. This might be important if thermodynamic gradients can evolve in the island region. Otherwise, as in steady state cases, only the particle and heat flux source/sink terms in the island region have to be considered in order to correctly compute balances. Second, we have referred to a single helicity island region so that the plasma flux-surface functions (the pressure, for instance) have one value in all the

separatrix. The transformation would equally apply to a fully chaotic region enclosed by the flux surfaces $\Phi_-$ and $\Phi_+$, to which a flux $\Phi_\mathrm{I}$ would be associated, because the same condition of having equal values of the pressure holds despite not having a separatrix. Thus, the plasma profiles would be continuous as required after the transformation Eq. 4.

### *2.3. Comparison between the metrics from the annular model and from Poincaré plots*

Here we compare island-free magnetic configurations with themselves after being perturbed so as to open magnetic islands. We calculate numerically the magnetic fields and obtain the flux-surface coordinate and FSA metric coefficients from Poincaré maps at several toroidal locations. Since, as discussed above, it is customary identifying $\bar{\rho}_0$ with the ideal unperturbed coordinate $\rho_0$, i.e. $\rho_0 \equiv \bar{\rho}_0$, from now on we simplify the notation by calling $\rho_0$ the flux-surface coordinate without islands. As before, we drop the notation for FSA and write directly $g^{\varrho\varrho}$ for the diagonal FSA metric coefficients referred to whatever radial coordinate.

*2.3.1. TJ-II equilibria and metric from Poincaré plots* Flux-surface coordinates for TJ-II magnetic configurations are routinely obtained from a set of codes and libraries previously confronted with magnetic surface mapping experiments [15]. Results from these codes will be referred to as "g3d". This suite of codes, however, is not prepared to obtain metric coefficients inside the island regions. A new code has been recently developed to obtain metric coefficients for a given magnetic field, also based on fitting Poincaré maps at several toroidal cuts [16]. We have chosen a vacuum magnetic configuration with $\iota = 3/2$ around mid-plasma radius. Its Poincaré section at the toroidal angle $\varphi = 0$ is plotted in Fig. 3 (a), corresponding to a calculation of the magnetic field starting from 29 points in major radius $R$ along the midplane ($Z = 0$) and following the field lines for 600 turns around the torus without assuming any symmetry (1-field period).

Adding a small error field to the configuration shown in figure 3 (a) we obtain the Poincaré section shown in figure 3 (b), where the existence of the low-order $\iota = 3/2$ in the unperturbed configuration promotes the onset of a vacuum $m = 2$ island chain. The FSA metric coefficients of the main plasma have been reconstructed following [16] in the two regions with flux surfaces outside the islands. A known property of TJ-II magnetic configurations is the linear relation between toroidal flux and enclosed volume, $\Phi(\rho_0) \propto V(\rho_0)$. Based on this property, also checked here, $V$ has been used instead of $\Phi$ in equation 2 to define the radial coordinate and then the metric from Poincaré plots. The relationship $\rho(\rho_0)$ thus obtained is shown in fig. 4 in green and magenta, respectively for the inside and outside regions. The piecewise transformation is evidenced by the gap in $\rho_0$ occupied by the island region. The original volume as a function of the new coordinate $\rho$ is discontinuous, but the new volume for transport calculations is the dashed line obtained after taking away the offset due to the missing island volume. The figure also shows the continuous derivative $\mathrm{d}V/\mathrm{d}\rho$ and the discontinuous FSA coordinate gradient. Next we proceed to compare these numerical results with the model.

*2.3.2. Comparison* The evident advantage of the annular model is that, in order to do 1D transport, all we need is an estimate of the width $\Delta$ that suits the opening

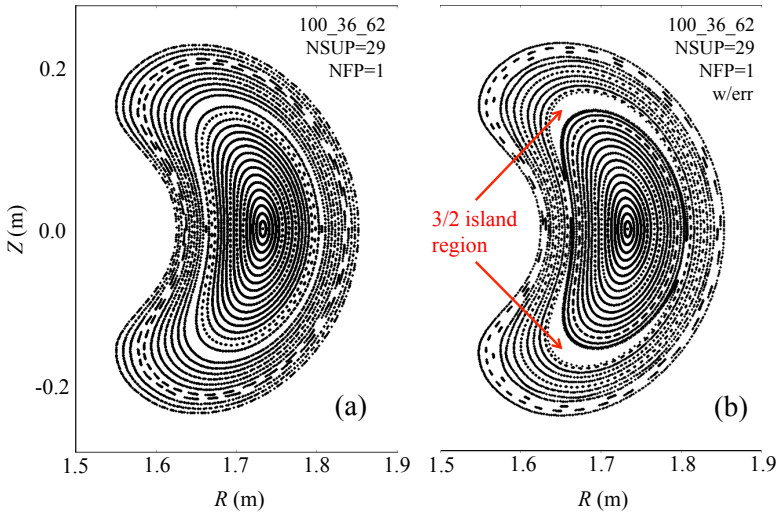


**Figure 3.** Poincaré plot at toroidal angle $\varphi = 0$ for a TJ-II vacuum configuration without (a) and with (b) error field to promote the opening of $m = 2$ islands around the $\iota = 3/2$ magnetic resonance. The maximum relative error in the magnitude of the magnetic field at the magnetic axis is 0.017%.

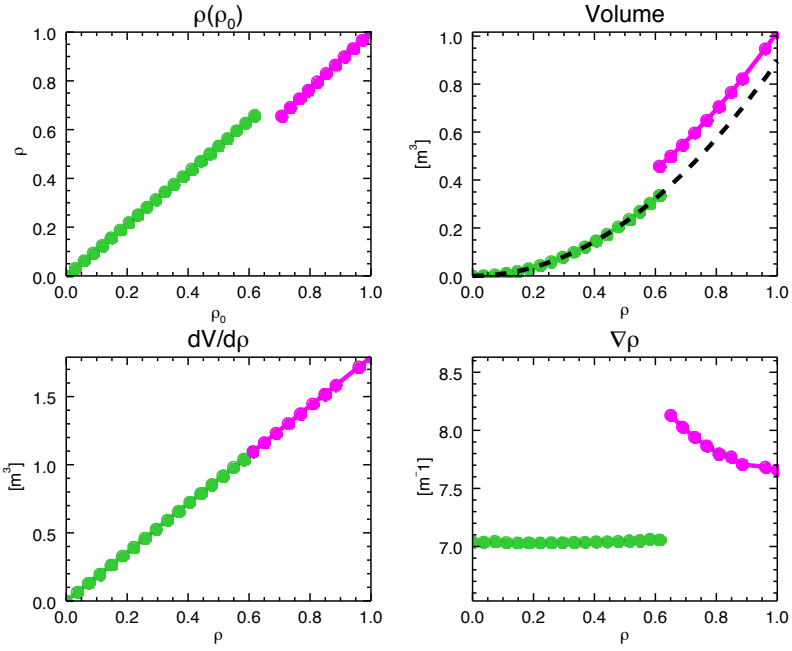


**Figure 4.** FSA quantities reconstructed from Poincaré plots at the inside (before the inside part of the separatrix, green) and outside (after the outside part of the separatrix, magenta) plasma regions. The volume in the new coordinate $\rho$ is represented with a dashed line.

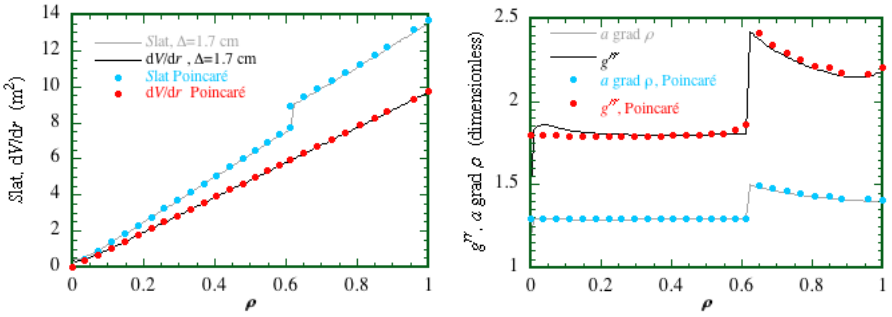


**Figure 5.** Comparison between $\mathrm{d}V/\mathrm{d}r$, $S_{\mathrm{lat}} = \mathrm{d}V/\mathrm{d}r|\nabla r|$ (left), $|\nabla r|$ and $g^{rr}$ (right) computed using the analitical annular model with island width $\Delta = 1.7$ cm (continous lines) and from the Poincaré plot with islands in figure 3 (dots). NB: $r \equiv a\rho$ has been used, e.g. $\mathrm{d}V/\mathrm{d}r = (1/a)\mathrm{d}V/\mathrm{d}\rho$.

of islands in perturbed MHD equilibria; on the other side the method from Poincaré plots is more precise, mainly near the resonant layer where there is some deformation of the flux surfaces. We now compare the FSA metric values obtained from Poincaré plots (figure 4) with the annular model of Section 2.

In figure 5, colored dots are related to the metric extracted from the Poincaré sections with islands (figure 3b), while continuous lines refer to the annular model applied on the unperturbed configuration (figure 3a). More precisely, an island width of $\Delta = 1.7$ cm has been assumed in equation 9 for the transformation 4, where $\rho_0$ is the radial coordinate obtained from the Poincaré plot without islands in figure 3 (a). Note that the maximum width of the islands shown in figure 3 (b) is about 2.8 cm, which would give an average value around 1.8 cm under a sine angular distribution of amplitudes. Therefore, the $\Delta$ value in the model that fits the metric obtained from the Poincaré plots with islands remains rather intuitive in terms of "effective island width" in laboratory coordinates.

Discontinuities in the metric magnitudes shown in figures 4 and 5 are very similar to the pure cylindrical case based on taking away the annulus in figure 1 [14]. The reason is that, in both cases, the origin of the discontinuities is the dilatation factor $\gamma$ (Eq. 6) due to having removed the plasma region corresponding to the island chain. The effect of the deformation of the magnetic flux surfaces near the resonant layer is quite small, in part due to the FSA process. It can be appreciated as slight increments near the discontinuity in the diagonal metric coefficient computed from Poincaré plots. Note that in figure 5 we use $g^{rr} = a^2 g^{\rho\rho} = a^2 \langle \nabla\rho \cdot \nabla\rho \rangle$ in order to ease the comparison with a purely cylindrical case, for which $g^{rr}_{\mathrm{cyl}} = 1$.

We can conclude that, at least in TJ-II magnetic configurations, the change in FSA metric is dominated by the removed volume, which renders the annular approximation quite accurate. Therefore, we may choose the metric from Poincaré plots for detailed studies where the magnetic topology can be considered fixed. On the other hand, since the annular model captures well the main geometrical changes, its simplicity makes it a very convenient tool for transport studies, particularly if the islands position and width change in time.

## 3. Examples of FSA transport with islands

We have just seen a good accordance between the FSA metric reconstructed from Poincaré plots of the perturbed configuration and from the analytical annular model applied on the unperturbed configuration. Removing the island region from the main plasma provokes discontinuities in the metric quantities, which must be dealt with in any transport code based on flux-surface averages. The numerical scheme may give a wrong evolution (i.e., also wrong steady states) depending on the numerical meshes used for the evolution equations and other details of the numerical scheme. Therefore, we begin by comparing a standard transport code using discontinuous metric profiles with another code that avoids the discontinuities at the expense of working in separate plasma domains.

### *3.1. Benchmark of the evolution with discontinuous fluxes*

Among many well-developed transport codes based on FSA quantities we have chosen the ASTRA shell [17], where the annular model metric can be easily implemented by means of a "plug-in subroutine" that modifies the metric coefficients in accordance with equations 4–6 and 8. The radial coordinate $\rho_0$ is here the unperturbed ASTRA radial coordinate, based on g3d data for TJ-II cases, and the island flux $\Phi_{\rm I}$ has been related to the "effective" island width through Eq. 9.

In order to assess the proper evolution of ASTRA despite the discontinuous radial fluxes, we need another transport code that can naturally include the geometry of magnetic islands. Such a code, MAxS, has been recently developed and compared in particular with ASTRA in cases without islands [18]. MAxS is a numerical implementation of the "multiple domain scheme": it evolves independently the transport equations in different plasma domains that communicate at each time step through appropriate boundary conditions. In the case of magnetic islands, the separatrix divides the plasma domains: the *inside* region, or core, from the main magnetic axis to the inside separatrix; the *outside* region from the external separatrix to the plasma edge, and the *island* region enclosed by the separatrix. A standard radial coordinate is defined in each domain. See [18] for details.

ASTRA and MAxS are run using a same transport model with identical initial conditions and metric profiles. The latter come from the unperturbed g3d metric modified by the annular model using an island width $\Delta = 1.7$ cm. For simplicity, only the transport equation

$$\partial_t \left( \frac{3}{2} n_e T_e \right) = (V' \langle g^{rr} \rangle \chi_e n_e T_e')' / V' + P_{e\rm NB}$$

is evolved with homogeneous diffusivity $\chi_e = 3$ m$^2$/s. It corresponds to the usual electron heat balance without convection. The prime means derivative with respect to the radial coordinate $r = a\rho$. Figure 6 shows the chosen, not evolving, profiles for electron density $n_e$ and power density deposition $P_{e\rm NB}$. The *inside* core (green) and *outside* (magenta) regions are shared by the two codes, whereas we set flat $n_e$ and $T_e$ initial profiles in the island region (only computed by MAxS) where the integrated $P_{e\rm NB}(r)$ is negligible. Since the metric of the island region is not important in this case, we take it cylindrical $g^{rr} = 1$. As can be seen in figure 7, ASTRA and MAxS converge to overlapping steady states for the evolving electron temperature. The

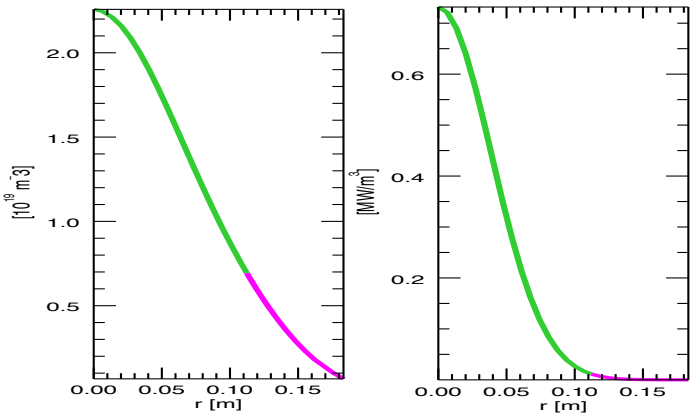


**Figure 6.** Profiles of electron density $n_e$ [$10^{19}$ m$^{-3}$] and heat source $P_{e\mathrm{NB}}$ [MW/m$^3$] used in MAxS and ASTRA in the inside (green) and outside (magenta) radial regions. The effective minor radius is $r = a\rho$.

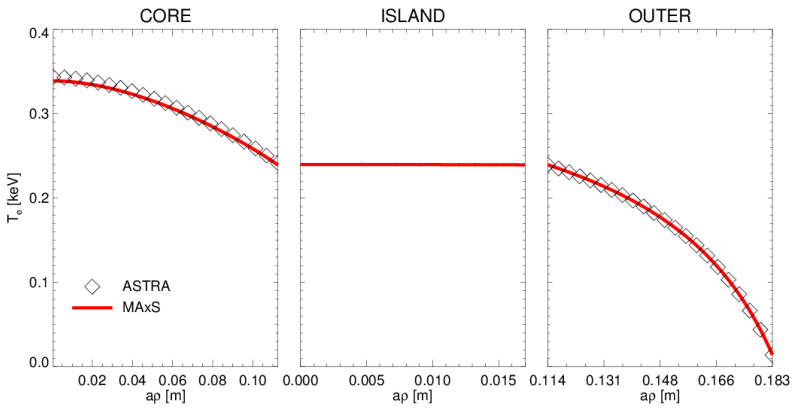


**Figure 7.** Overlapping steady state ASTRA (black) and MAxS (red) $T_e$-profiles in the core and outer regions. Since there is no power deposition in the island region, MAxS preserves the initial flat temperature.

main precaution is to set a high enough number of grid points in ASTRA (351 in these calculations) so the grid step size becomes much smaller than the island width.

We conclude that ASTRA can run using the annular model for transport analyses. We expect this to be the case also with any 1D transport code, as long as a similar checking is done to ensure that the discontinuities in the fluxes do not conflict with the numerical scheme. We recall that, even though we have always referred to eliminating island chains, the model basically eliminates an annular-like portion of plasma enclosed by well defined flux surfaces. This means that a chaotic region around the resonant layer would be treated equally from the geometrical perspective.

In what follows, we use ASTRA to propose transport studies in two helical plasmas with magnetic islands inside.

### *3.2. Geometrical effect of magnetic islands on transport in TJ-II plasmas with evolving rotational transform*

Here we present an example of predictive transport analysis in order to study how the opening of islands may affect the results due *only* to geometrical effects. The results are to be compared with well established results in TJ-II plasmas heated by EC-waves: low order rationals of $\iota$ leave a distinguishable trace in $T_e$-gradients when such "rationals" move through minor radius. This has been checked independently using Electron Cyclotron Emission (ECE) and Thomson Scattering diagnostics, and also different means of scanning the magnetic configuration (see [19] and references therein).

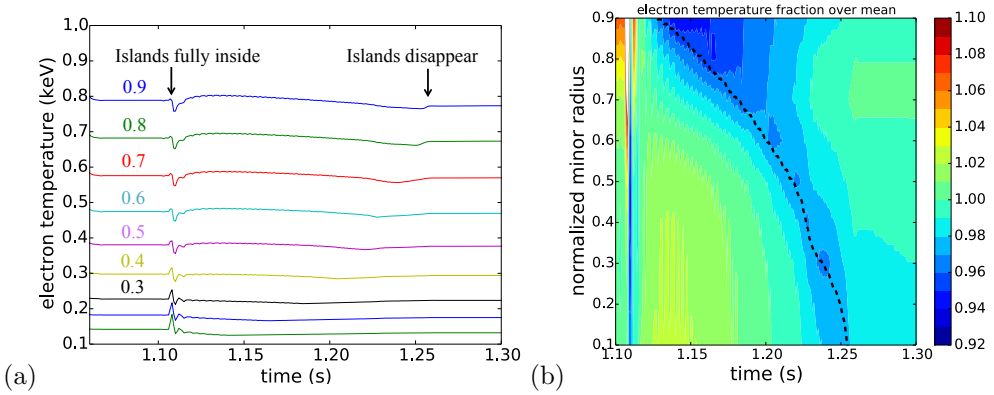


**Figure 8.** (a) Time traces of $T_e(\rho)$ for equally spaced $\rho$ values ranging from 0.1 to 0.9 in normalized minor radius during a simulated dynamic configuration scan; (b) evolution of the corresponding temperature profiles normalized to the time average. A dotted line represents the path followed by the $\iota = 8/5$ rational through minor radius during the scan.

We have set a transport model that mimics steady state $T_e$-profiles of ECH TJ-II plasmas for the given electron heat source and density profiles. In TJ-II experiments with variable magnetic configuration, the offset of the $\iota$-profile is changed continuously during the discharge so that selected rationals are moved through minor radius [20]. In the present case we move the $\iota = 8/5$ rational from edge to core during the simulated discharge. In order to make an island width that decreases with minor radius, we have set $\Delta = 1.5\rho$ cm, so the maximum effective width of 1.5 cm happens near the edge and decreases until collapsing at $\rho = 0$. Figure 8 (a) shows time traces of the simulated $T_e$ at different radial positions in the transformed $\rho$ coordinate. Initially, the islands are placed at $\rho = 0.975$ and there is just some loss of plasma volume but no discontinuity in the fluxes. At $t = 1.107$ s the islands are fully inside and the temperatures suffer a sharp change due to the sudden appearance of a discontinuous heat flux. During the time interval $1.107 < t < 1.257$ s the temperatures near the resonance tend to decrease; finally, when the rational $\iota = 8/5$ is outside the plasma ($t > 1.257$ s) the steady state is recovered and $\rho$ is equivalent to the unperturbed original coordinate $\rho_0$.

The evolution described above can be neatly visualized by following the evolution of the profile $T_e(\rho)/\bar{T}_e(\rho)$, where $\bar{T}_e$ is some reference profile, like the mean value during the whole time interval or the final profile in the absence of magnetic island. The result is qualitative the same, but we have chosen the time average to draw figure 8 because

this was done in the experiments [21], where the effect was found to be *opposite*: local temperatures above the mean follow the rational. Namely, the present exercise with the island-modified geometry indicates that the change in electron temperatures found experimentally should be related with an *improvement* of confinement, at or by the magnetic resonance, not by geometrical effects.

### *3.3. Consequences of energy sink at the island regions in LHD magnetic configurations*

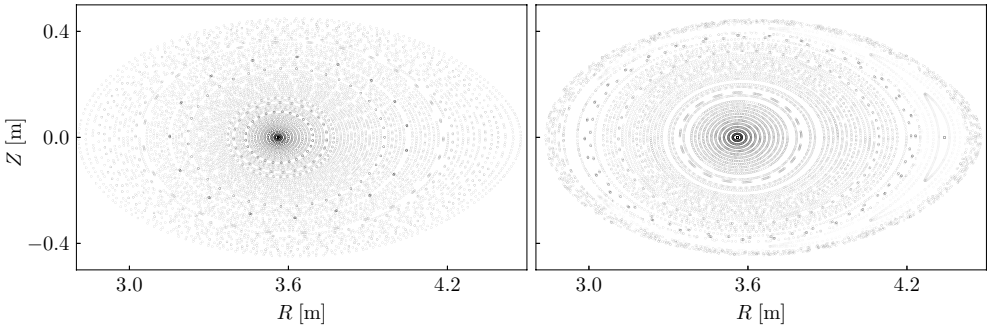


**Figure 9.** Poincaré plot of a low-$\beta$ LHD magnetic configuration (major radius $R_{\rm ax} = 3.6$ m) without (left) and with externally driven 1/1 island (right).

As a second example we present a case where data from a discharge with islands are to be analyzed in order to obtain information on transport outside the resonant zone. Several experiments in the LHD make use of the driven 1/1 island, which opens near the plasma edge as can be seen in figure 9. Here we show the Poincaré plots for two configurations, the unperturbed one where we define the coordinate $\rho_0$ (left) and the perturbed one that forces the opening of the near-edge island (right). For the latter case, realistic FSA metric coefficients for the different regions including the island have been reconstructed from Poincaré plots [16]. Therefore, we modify the coordinate $\rho_0$ related to the equilibrium configuration ($R = 3.6$ m) without islands using equations 4–6 and 8, and then obtain metric profiles to be compared with those reconstructed from the Poincaré plot of figure 9 (right). The comparison is shown in figure 10, where it is found that both the inner and outer regions are rather well approximated as long as a suited width ($\Delta = 7.6$ cm in this case) is chosen for the transformation. Note that the equatorial island width in figure 9 is about 12 cm.

In order to do transport analysis outside the resonant region we use the metric profiles from the annular model (figure 10). The starting, unperturbed configuration is obtained from VMEC giving rise to the normalized effective coordinate $\rho_0 \equiv r_{\rm eff}/a_{99}$, to which several diagnostics are referred. Here we transform the input kinetic profiles from Thomson Scattering data of LHD discharge No. 140534 (figure 11 top) and take away the data that fall in the resonant region spanned by the horizontal arrow. The remaining data and coordinates are mapped onto the radial coordinate $\rho$, which eliminates the island part of the profiles thus rendering them continuous and monotonous, see figure 11 (bottom). We can now perform transport studies on these profiles.

The LHD discharge #140534 around $t = 4$ s corresponds to a base plasma

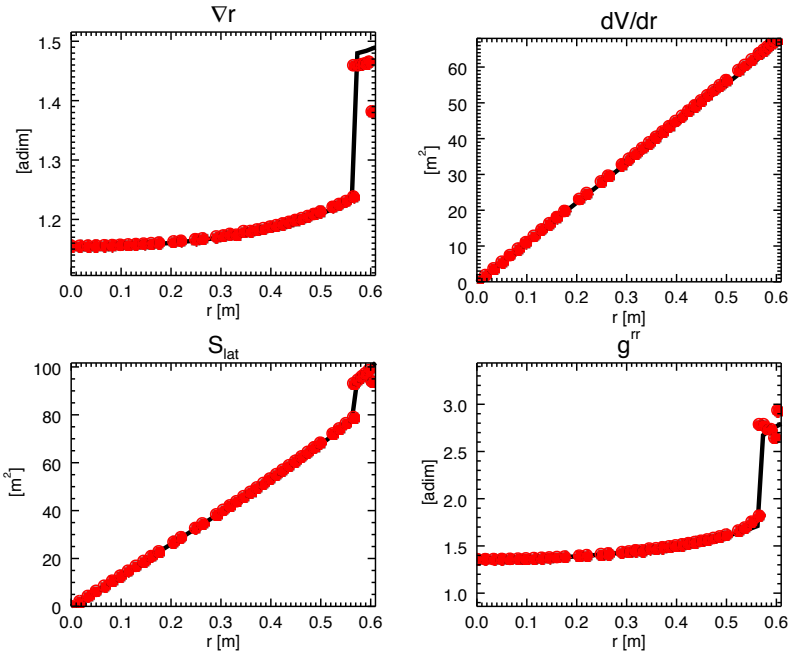


**Figure 10.** Comparison between $|\nabla r|$, $\mathrm{d}V/\mathrm{d}r$, $S_{\mathrm{lat}} = |\nabla r|\mathrm{d}V/\mathrm{d}r$ and $g^{rr}$ computed using the analytical annular model with $\Delta = 7.6$ cm (black line) acting on the metrics from the Poincaré plot in figure 9 (left), and the metrics directly from the Poincaré plot (red dots) with 1/1 island shown in figure 9 (right). As in figure 5, we define $r = a\rho$ where $a$ is a representative minor radius of the magnetic configuration.

sustained by NBI heating with superimposed modulated ECH (MECH) at 20 Hz with a square wave-form. We have set a diffusive transport model with neoclassical $\chi_e^{\mathrm{NC}}$ following the formulation used in [22], and a simple function $\chi_e^a = C\rho^8$ for the edge zone. Heat sources have not been calculated but taken as Gaussian profiles with different normalizations so as to obtain the respective heating powers of the selected discharge at $t = 4$ s (net NBI power $Q_{\mathrm{NBI}} = 15.8$ MW, ECH amplitude $Q_{\mathrm{ECH}} = 1.4$ MW). The widths and centering of the Gaussians have been adjusted so the source profiles are similar to those shown in [23]. Efficiency factors in the heating have been set so as to mimic the evolution of the experimental temperature at $R = 3.861$ m, corresponding to $\rho(\rho_0 = 0.27) = 0.3$ around $t = 4$ s, as shown in figure 12.

Heat pulse propagation experiments with localized central heating where the delay time is not monotonous with radius (e.g. [23]) are naturally reproduced with this model (outside the island region) because of the unique coordinate for the separatrix. If non-trivial transport calculations are necessary inside the island, they should be separately done as in [18]. A clear advantage of the annular model is that we can study the possible effect of other islands in MECH experiments without the need of re-calculating the metrics from Poincaré plots. Once the $T_e$ response to MECH is fairly reproduced (figure 12), we investigate a possible effect of opening islands around mid-radius due to the resonance $\iota = 1/2$, for instance as in [24]. Taking this latter reference as example, we use the annular model to change the island position: without re-doing the Poincaré sections we set an effective island width of 5 cm at the location

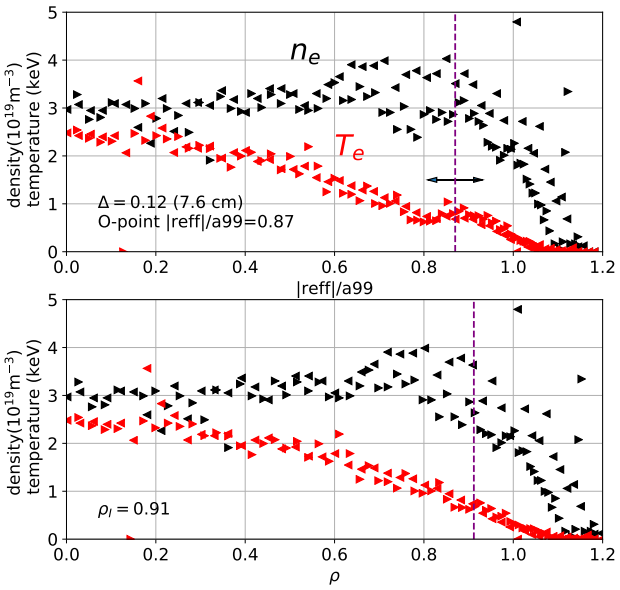


**Figure 11.** Thomson Scattering electron density (black) and temperature (red) profiles for LHD discharge #140534 at $t = 4$ s. Top: original data from negative (◀) and positive (▶) Thomson radius in the normalized coordinate $|r_{\rm eff}/a_{99}|$. A vertical dashed line indicates the center of the $\iota = 1$ resonance and a double-arrow its width $\Delta$. Error bars are not drawn for clarity. Bottom: The same data after eliminating the resonant region through the transformation Eq. 4. The location of the separatrix (vertical dashed line) has a new effective radius.

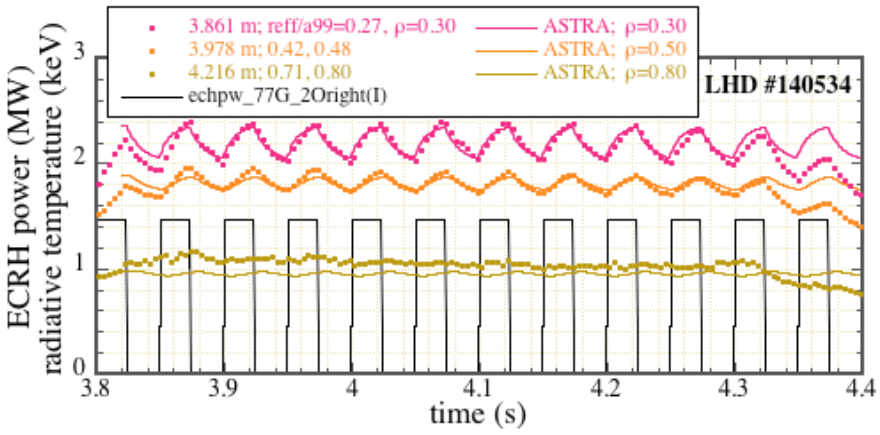


**Figure 12.** Time traces of the electron temperature around $t = 4$ s for LHD discharge #140534 (dots) and calculated values using ASTRA (lines). The labels show the corresponding laboratory coordinate $R$, the original $\rho_0 = r_{\rm eff}/a_{99}$ and the transformed $\rho$ according to figure 11. The modulated ECH power is shown with black lines.

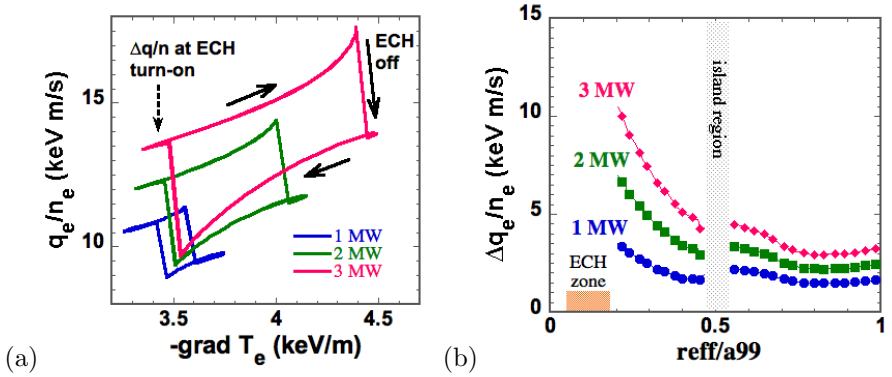


**Figure 13.** (a) Flux-gradient relation at $\rho = 0.6$ according to Eq. 13 for a transport simulation with heat source Eq. 14 at three different nominal ECH powers. (b) Corresponding profiles, in terms of the radial coordinate $\rho_0 \equiv r_{\rm eff}/a$, of the jump at the time of ECH turn-on.

of $\iota = 1/2$, around mid-radius. As in [24], we use different amplitudes for the MECH power, from 1 to 3 MW, with narrow Gaussian centered around $\rho = 0.1$. Then we set a diagnostic for the "experimental" heat flux normalized by the electron density at $\rho$,

$$\frac{q_e^{\rm exp}}{n_e}(\rho) = -\frac{1}{n_e S}\int_0^\rho {\rm d}\rho V' \left[\frac{3}{2} n_e \partial_t T_e - P_{\rm ECH} - P_{\rm NBI}\right] \tag{13}$$

Here all magnitudes, electron density $n_e$, temperature $T_e$, power densitites, area $S$ of the flux surface and $V' = {\rm d}V/{\rm d}\rho$, are profiles. $P_{\rm ECH}$ is a *nominal* ECH power under the assumption of 100% absorption.

Inspired by TJ-II results on the effects of ECH on the electrons, in the present exercise we hypothesize that the electron heat balance includes two heat sinks: one is due to direct ripple losses at the injection region, which basically is a correction to the nominal deposited power $\eta_{\rm rl} P_{\rm ECH}$ with $\eta_{\rm rl} < 1$ [25]; another one corresponds to fast electrons that can accumulate with very long confinement time in the resonant zone [26], in our case related with $\iota = 1/2$ around $\rho_s \approx 0.5$. In terms of transport, the latter provide a sink around the resonant region where the islands open. Even if these electrons are very few comparatively, their energies can be very high, say tens of keV, and thus represent a non-negligible power density sink $P_{\rm isl}$ for the plasma outside the islands zone. In order to account for these effects, in the transport calculations we set a source/sink term

$$P_e(\rho) = \eta_{\rm rl} P_{\rm ECH}(\rho) - P_{\rm isl}(\rho) \tag{14}$$

where $P_{\rm isl}(\rho)$ is a peaked function centered at $\rho_s$. This term, as all ECH power terms, is modulated as in figure 12.

Figure 13 (a) represents the flux-gradient relationship obtained using the diagnostic Eq. 13 for a simulation of the plasma with $P_e$ as in Eq. 14 using the same model for transport fluxes used in figure 12, i.e., a mostly neoclassical description of the electron heat transport except near the edge. The three closed curves correspond to the indicated simulated *nominal* ECH powers, $\int {\rm d}V P_{\rm ECH}$. Arrows indicate the evolution of the curve for the 3 MW case, which is qualitatively the same as the other curves. Each time the MECH is turned on there is a jump $\Delta q^{\rm exp}/n_e$ due to the unbalance between the time derivative term and the nominal power $P_{\rm ECH}$ in Eq. 13.

Such jump, as well as the covered range of $T_e$-gradients, increases with nominal power. The magnitude of the jump varies at each radial location giving rise to the profiles shown in Figure 13 (b) for the same cases in terms of the radial coordinate $\rho_0 \equiv r_{\rm eff}/a$ obtained with the inverse transformation 7. Outside the MECH zone, and considering a modulation period on the order of the energy confinement time, the jump is given by the excess power between the nominal $P_{\rm ECH}$ and $P_e$ in Eq. 14,

$$\Delta \frac{q_e^{\rm exp}}{n_e} \approx \int_0^\rho {\rm d}\rho V'[P_{\rm ECH} - P_e] = \int_0^\rho {\rm d}\rho V'[(1-\eta_{\rm rl})P_{\rm ECH} + P_{\rm isl}].$$

The calculations in the appropriate geometry allow for a quantitative estimate of these effects. In the case of figure 13 we have, for all cases, $\eta_{\rm rl} = 0.7$ and $\int {\rm d}V P_{\rm isl} = 0.3$ MW. The latter is responsible for the increment in $\Delta q^{\rm exp}/n_e$ when crossing the island region in figure 13 (b).

The present exercise has been developed as an application example of the transformations due to the annular model. Consequently, the transport analysis yielding figure 13 cannot be considered as representative of any particular LHD discharges. However, we see how the consideration of island regions may provide a contribution to experimental results as those shown in [24]. The consideration of the appropriate metric and estimates of the power density profiles, Eq. 14, should help to better quantify the effects attributed to turbulence in the experimental hysteresis loops.

## 4. Summary

1D transport analyses in toroidal plasmas where island chains are present can be done after eliminating the later from the transport domain. We have developed a coordinate change that reduces the problem to the region outside the islands, where a flux surface radial coordinate can be defined in the usual way, at the expense of having discontinuous radial fluxes. The resulting metric magnitudes (e.g. radial derivative of the volume, ${\rm d}V/{\rm d}\rho$, and FSA diagonal metric coefficient, $g^{\rho\rho}$) agree well with the values obtained directly from Poincaré plots if a proper effective island width is provided. By comparison with a transport code based on a Multiple Domain Scheme, and therefore free from discontinuities, we have also checked that a 1D transport code (ASTRA in our case) can handle the discontinuous fluxes satisfactorily. Finally, we have worked application examples considering two types of helical device: the TJ-II Heliac, where we find that the geometrical effects alone cannot explain the experimental observations when the islands move throughout minor radius in ECH plasmas; and the LHD Heliotron, where we propose an exercise to quantify the heat losses that would give rise to discontinuous flux-gradient relations in plasmas with modulated ECH in presence of an island region acting as a heat sink.

## Acknowledgments

This work has received funds from the Spanish Government via project ENE2014-52174-P and mobility grant PRX17/00425. This work has been carried out within the framework of the EUROfusion Consortium and has received funding from the Euratom research and training programme 2014-2018 under grant agreement No 633053. The views and opinions expressed herein do not necessarily reflect those of the European Commission.

## References


[1] Grad H 1967 *Physics of Fluids* **10** 137–154

[2] Hirshman S P and Whitson J C 1983 *The Physics of Fluids* **26** 3553–3568 (*Preprint* http://aip.scitation.org/doi/pdf/10.1063/1.864116) URL http://aip.scitation.org/doi/abs/10.1063/1.864116

[3] Shaing K, Tsai T, Chu M and Sabbagh S 2011 *Nuclear Fusion* **51** 043013 URL http://stacks.iop.org/0029-5515/51/i=4/a=043013

[4] Lopes-Cardozo N J, Hogeweij G M D, de Baar M, Barth C J, Beurskens M N A, Luca F D, Donné A J H, Galli P, van Gelder J F M, Gorini G, de Groot B, Jacchia A, Karelse F A, de Kloe J, Kruijt O G, Lok J, Mantica P, van der Meiden H J, Oomens A A M, Oyevaar T, Pijper F J, Polman R W, Salzedas F, Schüller F C and Westerhof E 1997 *Plasma Physics and Controlled Fusion* **39** B303

[5] Razumova K A, Alikaev V V, Borschegovskii A A, Chistyakov V V, Dremin M M, Gorshkov A V, Kislov A Y, Kislov D A, Krylov S V, Lysenko S E, Myalton T B, Notkin G E, Poznyak V I, Pavlov Y D, Roy I N, Savrukhin P V, Sushkov A V, Sannikov V V, Soldatov S V and Vershkov V A 2000 *Plasma Physics and Controlled Fusion* **42** 973

[6] Austin M E, Burrell K H, Waltz R E, Gentle K W, Gohil P, Greenfield C M, Groebner R J, Heidbrink W W, Luo Y, Kinsey J E, Makowski M A, McKee G R, Nazikian R, Petty C C, Prater R, Rhodes T L, Shafer M W and Van Zeeland M A 2006 *Physics of Plasmas (1994-present)* **13** 082502

[7] Misguich J H, Reuss J D, Constantinescu D, Steinbrecher G, Vlad M, Spineanu F, Weyssow B and Balescu R 2002 *Plasma Physics and Controlled Fusion* **44** L29

[8] Castejón F, Fujisawa A, Ida K, Talmadge J N, Estrada T, López-Bruna D, Hidalgo C, Krupnik L and Melnikov A 2005 *Plasma Physics and Controlled Fusion* **47** B53 URL http://iopscience.iop.org/article/10.1088/0741-3335/47/12B/S05/pdf

[9] Brakel R and the W7-AS Team 2002 *Nuclear Fusion* **42** 903

[10] Vargas V I, López-Bruna D, Herranz J, Castejón F and the TJ-II Team 2007 *Nuclear Fusion* **47** 1367 URL http://iopscience.iop.org/article/10.1088/0029-5515/47/9/039

[11] López-Bruna D, Estrada T, Medina F, de la Luna E, Romero J A, Ascasíbar E, Castejón F and Vargas V I 2008 *EPL (Europhysics Letters)* **82** 65002 URL http://stacks.iop.org/0295-5075/82/i=6/a=65002

[12] Lorenzini R, Alfier A, Auriemma F, Fassina A, Franz P, Innocente P, López-Bruna D, Martines E, Momo B, Pereverzev G, Piovesan P, Spizzo G, Spolaore M and Terranova D 2012 *Nuclear Fusion* **52** 062004

[13] Peraza-Rodríguez H, Sánchez R, Geiger J, Reynolds J and Tribaldos V 2014 Application of the siesta code to the calculation of mhd equilibria for the wendelstein 7-x stellarator *41st EPS Conference on Plasma Physics* (Berlin: European Physical Society) p P2.072 URL http://ocs.ciemat.es/EPS2014PAP/pdf/P2.072.pdf

[14] López-Bruna D, Momo B and Zhang Y 2017 One-dimensional treatment of the effect of small magnetic islands on transport in the TJ-II stellarator Tech. Rep. 1402 Laboratorio Nacional de Fusión por Confinamiento Magnético, CIEMAT

[15] López-Fraguas A, Ascasíbar E, Romero J A, García-Cortés I, Jiménez J A, Sánchez A L, Qin J, Otte M and TJ-II Team 2002 Magnetic surface mapping in TJ-II heliac *Proc. 13th International Stellarator Workshop* (Canberra, Australia) p PI.6 URL http://wwwrsphysse.anu.edu.au/admin/stellarator/papers/LFraguas_PI6.pdf

[16] Predebon I, Momo B, Suzuki Y and Auriemma F 2018 *Plasma Physics and Controlled Fusion* URL http://iopscience.iop.org/10.1088/1361-6587/aaaa49

[17] Pereverzev G V and Yushmanov P N 2002 ASTRA Automated System for TRansport Analysis Tech. Rep. IPP 5/98 Max Plank Institut für Plasmaphysik, Garching

[18] Auriemma F, López-Bruna D, Lorenzini R, Momo B, Predebon I, Suzuki Y, López-Fraguas A, Narushima Y, Sattin F, Terranova D and Zhang Y 2018 *Nuclear Fusion (submitted)*

[19] López-Bruna D, Vargas V I and Romero J A 2015 *Journal of Physics: Conference Series* **591** 012013 URL http://stacks.iop.org/1742-6596/591/i=1/a=012013

[20] López-Bruna D, Romero J, Jiménez-Gómez R, Pedrosa M, Ochando M, Estrada T, López-Fraguas A, Medina F, Herranz J, Kalhoff T, Ascasíbar E, de la Peña A, Lapayese F and Alonso J 2009 *Nuclear Fusion* **49** 085016 URL http://stacks.iop.org/0029-5515/49/i=8/a=085016

[21] López-Bruna D, Pedrosa M A, Ochando M A, Estrada T, van Milligen B P, López-Fraguas A, Romero J A, Baião D, Medina F, Hidalgo C *et al.* 2011 *Plasma Physics and Controlled Fusion* **53** 124022 URL http://iopscience.iop.org/article/10.1088/0741-3335/53/12/124022/meta

[22] Garcia J, Dies J, Castejon F and Yamazaki K 2007 *Physics of Plasmas* **14** 102511 (pages 10)
[23] Ida K, Inagaki S, Suzuki Y, Sakakibara S, Kobayashi T, Itoh K, Tsuchiya H, Suzuki C, Yoshinuma M, Narushima Y, Yokoyama M, Shimizu A, Itoh S I and the LHD Experiment Group 2013 *New Journal of Physics* **15** 013061
[24] Inagaki S, Tokuzawa T, Tamura N, Itoh S I, Kobayashi T, Ida K, Shimozuma T, Kubo S, Tanaka K, Ido T, Shimizu A, Tsuchiya H, Kasuya N, Nagayama Y, Kawahata K, Sudo S, Yamada H, Fujisawa A, Itoh K and the LHD Experiment Group 2013 *Nuclear Fusion* **53** 113006 URL http://stacks.iop.org/0029-5515/53/i=11/a=113006
[25] Ochando M A, Medina F and the TJ-II Team 2003 *Plasma Physics and Controlled Fusion* **45** 221 URL http://iopscience.iop.org/article/10.1088/0741-3335/45/3/304/pdf
[26] Ochando M A, Medina F, Rodríguez-Rodrigo L, Pedrosa M A, Hidalgo C and the TJ-II Team 1999 Confinement of fast electrons at rational surfaces in the TJ-II stellarator *Proc. 12th IAEA Int. Stellarator Workshop* (Madison (WI) USA) URL http://www-fusion.ciemat.es/sw2005/conferences/madison99/papers/Ochando.pdf